Progress In Electromagnetics Research B, Vol. 100, 133–154, 2023

Independent Control Over Passbands in Highly Selective and Compact Triple-Band Bandpass Filter Based on Substrate Integrated Waveguide

Soumit S. Chaudhury[1, *], Seema Awasthi[2], and Rajat K. Singh[3]

Abstract—This paper proposes a method of independent control over each passband in a high performance triple bandpass filter, which is an essential requirement in the field of microwave communication systems. Individual techniques are presented here to control the excited modes that are responsible for the generation of triple passbands based on substrate integrated waveguide loaded with semi-circular mushroom resonators. Initially, a circular substrate integrated waveguide (CSIW) loaded with two cascaded semi-circular mushroom resonators (ScMRs) with distinct modifications and orientations in the schematic is employed to generate three passbands. The fundamental mode and next higher order mode of the entire resonator structure are utilized to generate three passbands, and distinct techniques of mode perturbations and variation in coupling strength are introduced to independently control the excited modes. Subsequently, the methods established to control the excited modes are employed to independently control the center frequencies (CFs) of three passbands. All those methods established to control the CFs of the three passbands are verified with experimental results which show good agreement with the simulated ones.

1. INTRODUCTION

Multiple bandpass filters with the ability to control the passbands independently attract significant attention in the field of microwave communications systems. In present days of microwave engineering, along with independent control over the passbands, the common requirements from a reconfigurable multiple bandpass filter are high Q-factor, low insertion loss in the passbands, high selectivity in the frequency response, compact size, and easy integration with planar circuits. Several research groups have made significant developments in Substrate Integrated Waveguide (SIW) technology in order to attain the characteristics of high performance filters [1–3]. Several researchers have utilized the advantages of SIW to implement multiple bandpass filters and have proposed specific techniques to control the generated passbands. SIW based inverter coupled resonators are presented to develop triple bandpass filter having quasi-elliptic frequency response [4]. Triple bandpass filters based on a SIW cavity are presented, where multiple mode excitations are utilized after introducing the mode perturbation technique using metallic vias in the cavity, but the passbands suffer from high insertion loss and poor selectivity, and the cavities occupy large size [5, 6]. Apart from mode perturbation technique, dual mode resonances and split type dual band symmetrical frequency response are generated using coupling topologies to present triple passband filters, but the cavities are of large size, and the coupling topology is also complex [7, 8]. In order to improve the selectivity and out-of-band response of the

Received 22 March 2023, Accepted 8 June 2023, Scheduled 19 June 2023
* Corresponding author: Soumit Samadder Chaudhury (soumit@ifheindia.org).
[1] Department of Electronics and Communication Engineering, Faculty of Science and Technology, ICFAI Foundation for Higher Education, Hyderabad, India. [2] Department of Electrical Engineering, Indian Institute of Technology Kanpur, Kanpur, India. [3] Department of Electronics and Communication Engineering, Indian Institute of Information Technology Allahabad, Allahabad, India.

frequency characteristics as further developments, composite right/left handed (CRLH) structures have been used to propose multiple bandpass filters along with miniaturized filter size [9–11]. The mushroom resonators, which are typical CRLH structures, have been employed to present the idea of independent control of passbands of multiple bandpass filters based on SIW cavity [12].

The process of reconfiguring the passbands in bandpass filters is explored and engineered by various groups of researchers. Serious developments regarding reconfiguration of center frequencies in SIW filters have been addressed in [13–16]. Independently reconfigurable dual-mode dual-band SIW filters with relatively less selectivity is proposed in [13]. Transmission lines with embedded switches are introduced in coupled resonators to implement a new topology which has helped to design a SIW bandpass filter with abilities to control the center frequencies of the passband [14]. Tuning elements such as lumped capacitors and varactor diodes are utilized several times very significantly to exploit the electric field intensity of SIW cavity in order to control the resonance frequencies of individual passbands [15, 16]. Normally, the controlling of passbands in multiple bandpass filters is realized using electrical, mechanical, and radio frequency microelectromechanical (RF-MEMS) tuning. Electric tuning elements are mostly preferred by researchers, due to their operational ease with controlling voltage used to control the CFs of multiple bandpass filters. Surface mount capacitors, stub capacitors, lumped capacitors, and piezoelectric actuators are some fascinating electric tuning elements used to control the CFs of the passbands [17–27]. The criticality of these tunable bandpass filters lies in the implementation of their electric tuning elements which are sometimes quite complex and hard to operate [17, 19, 22, 23, 26, 27]. The passbands of multiple bandpass filters mostly suffer high insertion losses when the CFs are controlled by electrical tuning elements [17, 18, 20, 22, 27]. Apart from electrical elements, RFMEMS devices are too used to control the CFs and bandwidths (BWs) of passband filters based on SIW technology [28, 29]. Although the CFs achieve a wide range of tuning, the passband undergoes significant insertion loss especially at the middle of tuning range [28, 29]. Researchers have furthermore developed the process to control the CFs of the passbands based on mechanical tuning [30–32]. Multiple screws are introduced into the additional vias in the SIW cavity resonator, and such metallic flanges are implemented in order to control the passbands both in common mode and in differential mode with low insertion loss [32]. Till now the control over passbands is implemented mostly on single bandpass filters [17–19, 21, 22, 24–32]. Some developments are obviously proposed where independent control over passbands is achieved on dual and multiple bandpass filters [20, 23, 33–35]. Apart from electrical or mechanical tuning, the controlling over passbands is also realized by introducing complementary split ring resonators (CSRRs) and perturbation slots in the resonating cavity [33–35]. These days, microwave communication systems generally welcome high performance multiple bandpass filters of higher order with low insertion loss in passbands and high selectivity in the passband frequency response along with the ability to control all the passbands independently. SIW cavity loaded with mushroom resonators can provide a flexible platform to propose multiple bandpass filters with the ability to control the passbands independently [9–12, 36, 37].

This paper presents a circular SIW cavity loaded with two cascaded ScMRs in such a way that the three passbands generated by the resonating structures can be controlled independently after introducing certain parametric modifications in the loaded mushroom resonators and SIW cavity. The proposed filter is a 2nd order triple bandpass filter having high selectivity in the frequency response with six transmission zeros (TZs) and relatively low insertion loss in the passbands. An open CSIW cavity is created by removing a circular metallic patch from the upper conductor of the CSIW. Two cascaded semicircular mushroom resonators (ScMRs) electrically coupled to each other along their linear edges are loaded into the open cavity of CSIW. The microstrip transmission lines of $50\,\Omega$ characteristic impedance and the circular coupling slotlines which cover the peripheral boundary of the resonating structures with modified orientations are employed to excite the fundamental mode (TM_{101}) and the next higher order modes, i.e., (TM_{201odd}) and ($TM_{201even}$) modes, to generate the 1st, 2nd, and 3rd passbands, respectively. A source to load coupling and two cross couplings between different modes of the loaded ScMRs are formed to create all together six TZs throughout the frequency response of the filter passband. Consequently, the frequency response of the proposed filter becomes highly selective. Later on three separate techniques are implemented to independently control the center frequency (CF) of each passband. After studying the electric field distributions of the resonator at all three passbands, the CF of the 1st passband is controlled by changing the positions and dimensions of the ScMR vias

such that the electric field distribution of the fundamental mode (TM_{101}) is perturbed keeping the other excited modes undisturbed. Two different techniques are employed in order to control the CF of the 2nd passband, that too without disturbing the 1st and 3rd passbands. Firstly, linear perturbation slots with particular orientations are loaded into the mushroom resonators to disturb the surface current distribution in such a way that the 2nd excited mode is disturbed, and its resonance frequency shifts, but the 1st and 3rd modes remain as they are. Secondly, a pair of rectangular complementary split ring resonators (CSRRs) are loaded to each of the ScMRs with an orientation such that the split gaps of the CSRRs are positioned exactly at the region of maximum intensity of the electric field of the ScMRs. The change in dimensions of the loaded CSRRs affects the resonance frequency of the 2nd passband without disturbing the CFs of the 1st and 3rd passbands. The CF of the 3rd passband is independently controlled by the angular slotlines which cover the peripheral boundary of the ScMR loaded CSIW. The change in angular separation between the coupling slotlines affects the source to load coupling which shifts the center frequency of the 3rd passband keeping the 1st and 2nd passbands undisturbed.

The proposed work in the paper is sequenced as such that the idea of generating triple passbands by loading ScMRs in CSIW cavity is initially illustrated along with proper descriptions of coupling topology and electric field distributions at corresponding center frequencies. Thereafter, the method of independent control over the passbands is described with elaborate understandings of electric field distributions and surface current distributions at separate resonating frequencies of the excited modes along with the study of frequency responses of the corresponding passbands.

2. GENERATION OF TRIPLE PASSBAND USING SCMRS LOADED CSIW CAVITY

Two ScMRs with some particularly modified orientations are cascaded along their linear edges by maintaining a uniform slot gap. These cascaded ScMRs are loaded into a CSIW cavity after etching out a circular metal patch from the upper conductor of the CSIW cavity. Thereafter, the entire resonating structure is excited using capacitive coupled microstrip transmission lines of 50 Ω characteristic impedance and angular coupling slotlines circumfering the resonating structure. Thus three passbands are generated by exciting the fundamental mode (TM_{101}) and next higher order split modes, i.e., (TM_{201odd}) and ($TM_{201even}$).

2.1. Semi-Circular Mushroom Resonators (ScMRs)

Figure 1(a) shows the top view and 3D view schematic of a single element ScMR acting as the basic building element for this triple bandpass filter. The electric field distributions of this single element ScMR for mode 1 (TM_{101}), mode 2 (TM_{201}), and mode 3 (TM_{102}) are shown in Figure 1(b). Figure 2 shows two cascaded ScMRs facing each other along the linear edges and modeled on a 0.787 mm thick dielectric substrate, Rogers RT/Duroid 5880 having dielectric constant, $\varepsilon_r = 2.2$ and magnetic loss

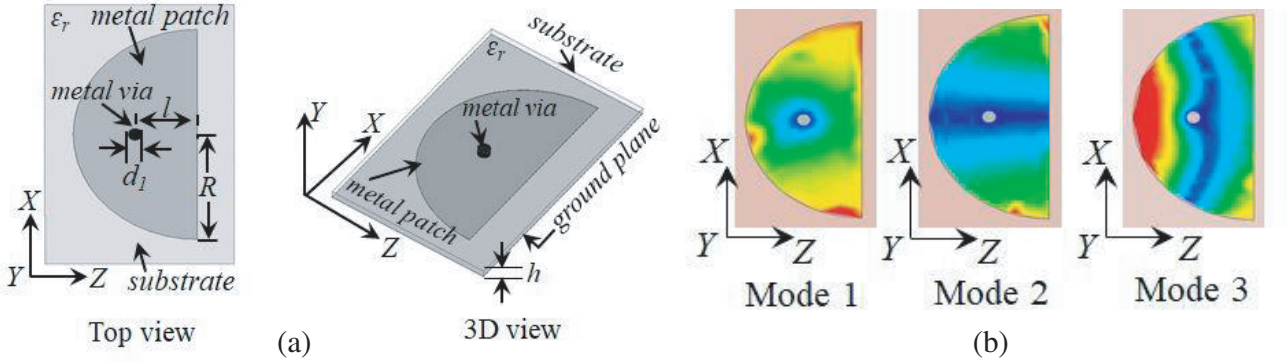

Figure 1. Single element ScMR and electric field distributions of mode 1, mode 2 and mode 3. (a) Single element ScMR with top view and 3D view and (b) Electric field distributions of mode 1 (TM_{101}), mode 2 (TM_{201}) and mode 3 (TM_{102}).

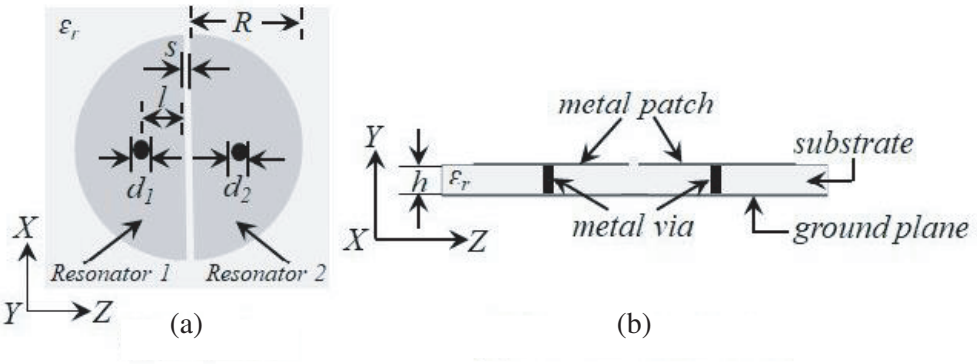

Figure 2. Schematic of two cascaded ScMRs. (a) Top view and (b) Cross sectional view.

tangent, $\tan\delta = 0.0009$. These two coupled ScMRs along their linear edges are utilized to generate 2nd order resonances at individual excited modes while realizing triple passbands.

2.2. ScMRs Loaded CSIW Cavity Based Triple Bandpass Filter

A circular metal patch is removed by etching out a portion of the upper conductor of CSIW cavity having via diameter, $d = 0.8\,\text{mm}$, angular separation between two consecutive vias with respect to cavity center, $\alpha = 5^\circ$ and distance between the edges of two diametrically opposite vias, $D = 41.4\,\text{mm}$, as shown in Figure 3(a). $(D - 2c)$ is the diameter of this etched out circular metal patch, where $c = 0.2\,\text{mm}$. Figure 3(b) shows that two cascaded ScMRs are loaded inside the CSIW cavity after etching out the circular metallic patch. Based on the factor of the guided wavelength (λ_g) the fundamental modes of

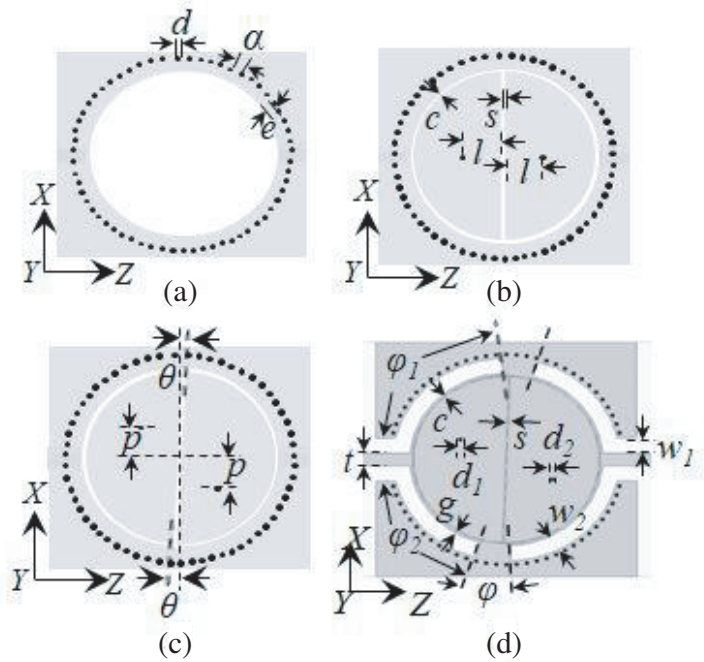

Figure 3. ScMRs with certain modifications are loaded into CSIW cavity. (a) CSIW cavity with etched out circular patch, (b) ScMRs loaded into CSIW cavity, (c) Loaded ScMRs subjected to certain modifications and (d) Entire triple-bandpass filter structure. Parametric values: $R = 17\,\text{mm}$, $d_1 = d_2 = 0.8\,\text{mm}$, $l = 8.5\,\text{mm}$, $s = 0.22\,\text{mm}$, $p = 3.8\,\text{mm}$, $\theta = 2^\circ$, $D = 41.4\,\text{mm}$, $c = 0.2\,\text{mm}$, $d = 0.8\,\text{mm}$, $\alpha = 5^\circ$, $e = 0.4\,\text{mm}$, $w_1 = 3\,\text{mm}$, $w_2 = 3\,\text{mm}$, $g = 0.45\,\text{mm}$, $\varphi = 25.7^\circ$, $\varphi_1 = 84^\circ$, $\varphi_2 = 70.3^\circ$.

resonance of the ScMRs are derived which are utilized to evaluate the dimensions of ScMR as well. The modal resonance frequencies determined from the eigen-mode analysis of the CSIW cavity help to determine the dimensions of it. Out of the three passbands generated, the 1st is formed due to the excitation of the fundamental mode (TM_{101}) whereas the 2nd and 3rd passbands are formed due to the higher order excited mode (TM_{201}) that is split into odd and even modes, i.e., (TM_{201odd}) and ($TM_{201even}$) modes, respectively. The loaded ScMRs assembled in cascaded fashion are innovated structurally by shifting the mushroom vias of $ScMR_1$ and $ScMR_2$ along X and $-X$ axes by a shift of $p = 3.8\,\text{mm}$ and $-3.8\,\text{mm}$, respectively, and later an angular rotation of $\theta = 2^\circ$ is rotated about an axis normal to the center of the circular SIW cavity. Figure 3(c) shows the modifications made in the structure of cascaded ScMRs, which is necessary to excite all three modes simultaneously as the linearly aligned microstrip transmission lines of $50\,\Omega$ characteristic impedance are not enough to excite these modes alone. A source to load coupling is also introduced in the coupling mechanism of the resonator structure, which is realized by extending the coupling slotlines circularly up to a certain angle as shown in the schematic of the entire filter structure in Figure 3(d).

The possibility of exciting the modes, which are responsible for the generation of three passbands, is assured after studying the electric field distributions of the structurally modified single ScMR as shown in Figure 4. The optimized values of the geometric parameters are shown in the caption of Figure 3. Considering those values, the filter structure is modeled on a 0.787 mm thick dielectric substrate, Rogers RT/Duroid 5880 having dielectric constant, $\varepsilon_r = 2.2$ and magnetic loss tangent, $\tan\delta = 0.0009$ and simulated using Ansoft HFSS 17. The frequency response is shown in Figure 5, which shows that the three passbands generated by exciting TM_{101}, TM_{201odd}, and $TM_{201even}$ modes have center frequencies (CFs) at 1.8 GHz, 3.5 GHz, and 4.3 GHz, respectively. Highly selective frequency response of triple bandpass filter is observed after generating six TZs throughout the passband as shown in Figure 5. The source to load coupling creates two TZs, TZ_1 at 1.7 GHz and TZ_6 at 4.8 GHz, which lie at the lower stopband and upper stopband of the entire filter passband [38]. Two different cross couplings between the excited modes of the loaded ScMRs are utilized to generate two TZs each between the 1st and 2nd passbands and between the 2nd and 3rd passbands [38]. Figure 6 shows the coupling topology used for the proposed filter which illustrates that the source is directly coupled to TM_{101}, TM_{201odd}, and $TM_{201even}$ modes of $ScMR_1$, and these modes of $ScMR_2$ are directly coupled to load. Direct couplings between the individual excited modes of TM_{101}, TM_{201odd}, and $TM_{201even}$, between the two ScMRs are employed to create the 1st, 2nd and 3rd passbands, respectively. As shown in Figure 6, the cross coupling created between the fundamental mode (TM_{101}) of $ScMR_1$ and TM_{201odd} mode of $ScMR_2$ and additionally the cross coupling created between TM_{201odd} mode of $ScMR_1$ and fundamental mode (TM_{101}) of $ScMR_2$, all together generate two TZs, i.e., TZ_2 and TZ_3 between the 1st and 2nd passbands. Similarly, the other two TZs, i.e., TZ_4 and TZ_5, generated between the 2nd and 3rd passbands are due to a separate cross coupling based on the coupling topology shown in Figure 6. The frequencies of transmission zeros (TZs), TZ_1 and TZ_6, formed due to the source to load coupling can be evaluated using the elements of the coupling matrix shown in Equation (1) and formed by the coupling topology

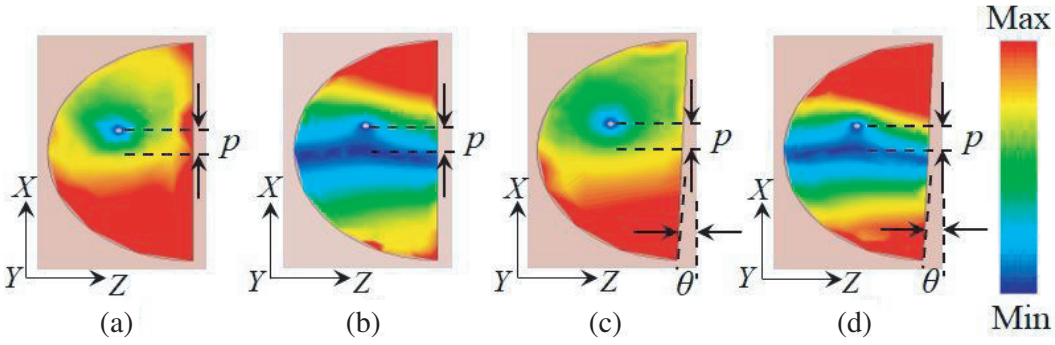

Figure 4. Electric field distributions of a ScMR. (a) TM_{101} mode with via shifted by p, (b) TM_{201} mode with via shifted by p, (c) TM_{101} mode with via shifted by p and ScMR rotated by angle θ and (d) TM_{201} mode with via shifted by p and ScMR rotated by angle θ.

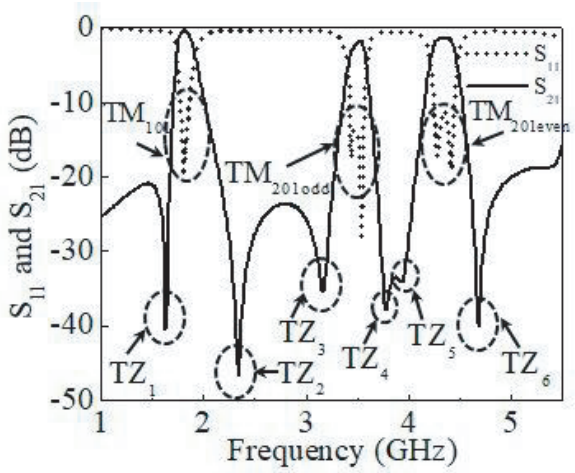

Figure 5. Simulated frequency response of S-parameters.

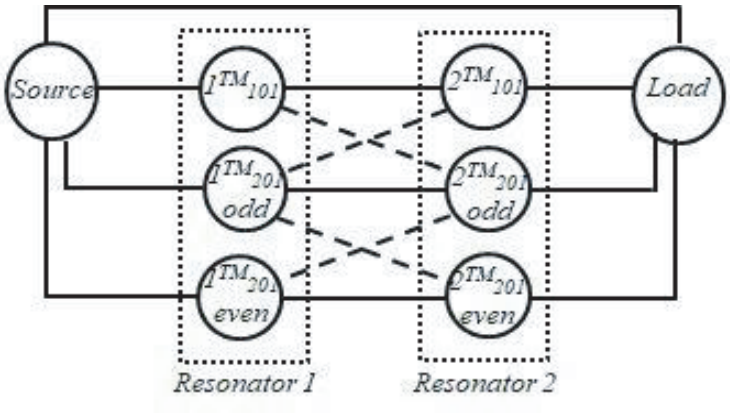

Figure 6. Coupling topology of the triple-band bandpass filter.

as described in [39, 40].

$$M = \begin{bmatrix} \ddots & Source & 1 & 2 & Load \\ Source & 0.0 & 0.1566 & 0.0 & 0.0195 \\ 1 & 0.1566 & 0.0 & -0.1191 & 0.0 \\ 2 & 0.0 & -0.1191 & 0.0 & 0.5902 \\ Load & 0.0195 & 0.0 & 0.5902 & 0.0 \end{bmatrix} \tag{1}$$

These two TZs, TZ_1 and TZ_6, which are formed due to the source to load coupling are extracted from Equation (2), whose coefficients are used to form the coupling matrix.

$$M_{SL}\omega^2 + (M_{SL} - M_{12} - M_{2L})\,\omega + (M_{1S} + M_{LS} - M_{21}) = 0 \tag{2}$$

In Equation (2), ω is the frequency variable in the lowpass frequency domain, and the terms of the coefficients are the elements of the coupling matrix. The frequencies of TZ_1 and TZ_6 are extracted from this quadratic equation. As explained above, two TZs formed between the 1st and 2nd passbands and between the 2nd and 3rd passbands are split into two TZs from each of those due to the cross coupling of modes. According to the coupling topology, the frequencies of the TZs between the passbands are extracted from Equation (3) as expressed below [39, 40].

$$\omega = -\frac{M_{11}M_{S2}M_{L2} + M_{22}M_{S1}M_{L1}}{M_{S2}M_{L2} + M_{S1}M_{L1}} \tag{3}$$

The conventional optimization method for implementing multiple bandpass filter as described in [41] is employed to design this triple bandpass filter based on certain specifications. The 1st passband is specified with a center frequency (CF) of 1.8 GHz and 3 dB fractional bandwidth (FBW) of 9.3%; the 2nd passband is specified with a center frequency (CF) of 3.53 GHz and 3 dB fractional bandwidth (FBW) of 5.1%; and the 3rd passband is specified with a center frequency (CF) of 4.35 GHz and 3 dB fractional bandwidth (FBW) of 6%. The specified return loss for all three passbands is 15 dB. Figure 7 shows the electric field distributions and surface current distributions of the proposed filter structure at the three resonating modes that are excited to generate three passbands. The maximum electric field intensity of the fundamental mode (TM_{101}) is shifted along $-X$ axis and $+X$ axis in $ScMR_1$ and $ScMR_2$ respectively due to the shift in the mushroom vias as explained earlier and shown in Figure 7(a). Figure 7(b) and Figure 7(c) show the electric field distributions of TM_{201odd} and $TM_{201even}$ modes, where the mushroom vias lie nearly in the null region of electric field distributions. The electric field intensity maximizes at the edges of ScMRs along X axis in both TM_{201odd} and $TM_{201even}$ modes as shown in Figure 7(b) and Figure 7(c). The distributions of surface current at fundamental mode (TM_{101}) become intense near the mushroom vias, but the region of maximum intensity shifts according to the displacements of the mushroom vias as shown in Figure 7(d). In the higher order modes, i.e., at TM_{201odd} and $TM_{201even}$ modes, the surface current distributions intensify at the region where the intensity of electric field is minimum as shown in Figure 7(e) and Figure 7(f). The shifted mushroom vias lie at the region of surface current distribution with maximum intensity. This triple bandpass filter modeled on a 0.787 mm thick dielectric substrate, Rogers RT/Duroid 5880 having dielectric constant, $\varepsilon_r = 2.2$ and magnetic loss tangent, $\tan\delta = 0.0009$ is simulated in Ansoft HFSS 17. It occupies a compact area of $0.26\lambda_0 \times 0.26\lambda_0$, where λ_0 is the corresponding wavelength in vacuum for the fundamental mode (TM_{101}).

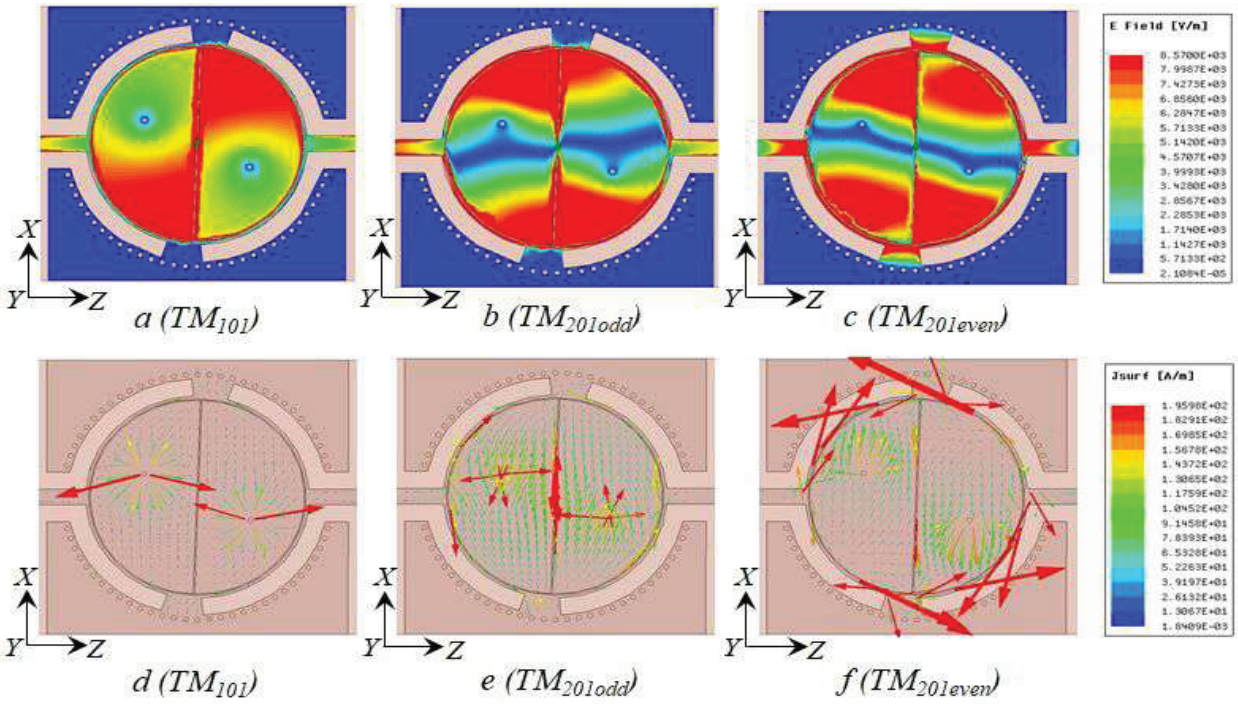

Figure 7. Electric field distributions and surface current distributions of the proposed filter structure. (a) Electric field distribution at TM_{101} mode, (b) Electric field distribution at TM_{201odd} mode, (c) Electric field distribution at $TM_{201even}$ mode, (d) Surface current distributions at TM_{101} mode, (e) Surface current distribution at TM_{201odd} mode and (f) Surface current distribution at $TM_{201even}$ mode.

3. INDEPENDENT CONTROL OVER EACH PASSBAND

Separate methods are proposed to control the excited modes which are responsible for the generation of three passbands in this triple bandpass filter. An attempt is carried out to independently control each passband without disturbing the other passbands. Possible care is taken in this process of mode controlling in order to maintain the selectivity of each passband by keeping the generated TZs undisturbed.

3.1. Control over 1st Passband

3.1.1. Control over 1st Passband by Displacing Mushroom Vias

Figure 7(a), Figure 7(b), and Figure 7(c) show the electric field distributions of the fundamental mode (TM_{101}) and next higher order modes (TM_{201odd} and $TM_{201even}$) of the filter structure. This field distribution clearly ensures that a linear displacement of the mushroom vias in an inclined direction as shown in the schematic in Figure 8(a) disturbs the electric field distributions of $TM_{101\,mode}$, while TM_{201odd} and $TM_{201even}$ modes remain undisturbed. The fabricated sample with linear displacements of the mushroom vias, $m = 5.2$ mm, is shown in Figure 8(b).

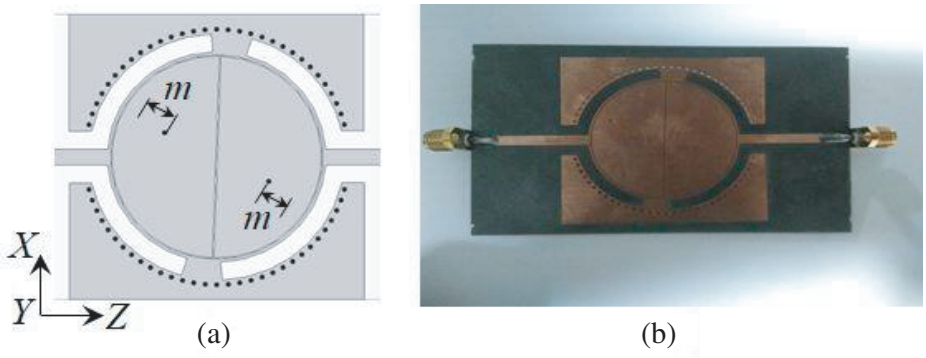

Figure 8. Schematic of the filter structure with inclined displaced mushroom vias. (a) The modeled filter structure. (b) The fabricated sample.

The mentioned fact is justified by studying the field distributions of three modes in Figure 9, where it is quite evident that the maximum field intensity in TM_{101} mode is shifted more towards the mushroom boundary at one end, but the field distributions in TM_{201odd} and $TM_{201even}$ modes remain nearly undisturbed due to such linear displacements in the mushroom vias.

In spite of such inclined displacements of vias, they lie in the null regions in TM_{201odd} and $TM_{201even}$ modes. Figure 10 shows the surface current distributions at the upper conductor of the structure for

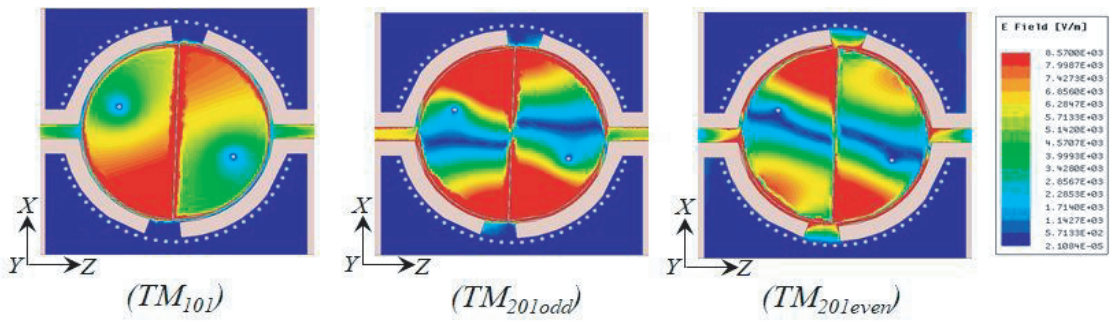

Figure 9. Electric field distributions of the filter structure with displaced mushroom vias in an inclined direction.

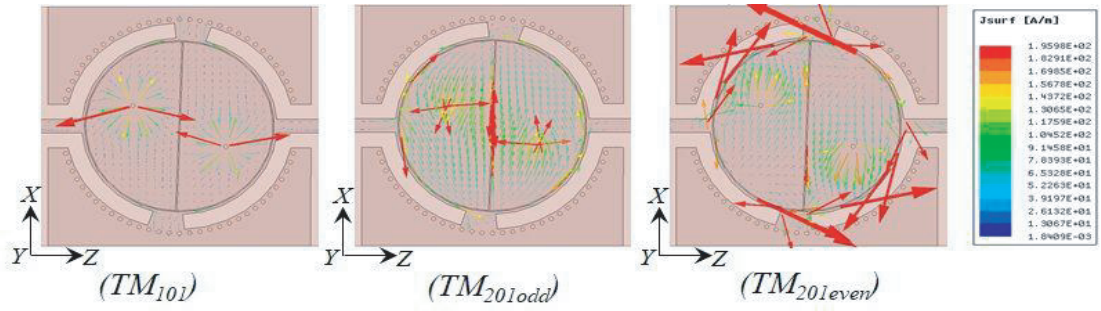

Figure 10. Surface current distributions of the filter structure with displaced mushroom vias in an inclined direction.

these three excited modes when the mushroom vias are linearly displaced in an inclined direction. This study of electric field and surface current distributions helps to anticipate the perturbations introduced in TM_{101} mode along with the unperturbed TM_{201odd} and $TM_{201even}$ modes. Therefore, a control over the fundamental mode (TM_{101}) is expected without disturbing the higher modes. The simulated frequency response of this triple bandpass filter with regular inclined displacements of mushroom vias

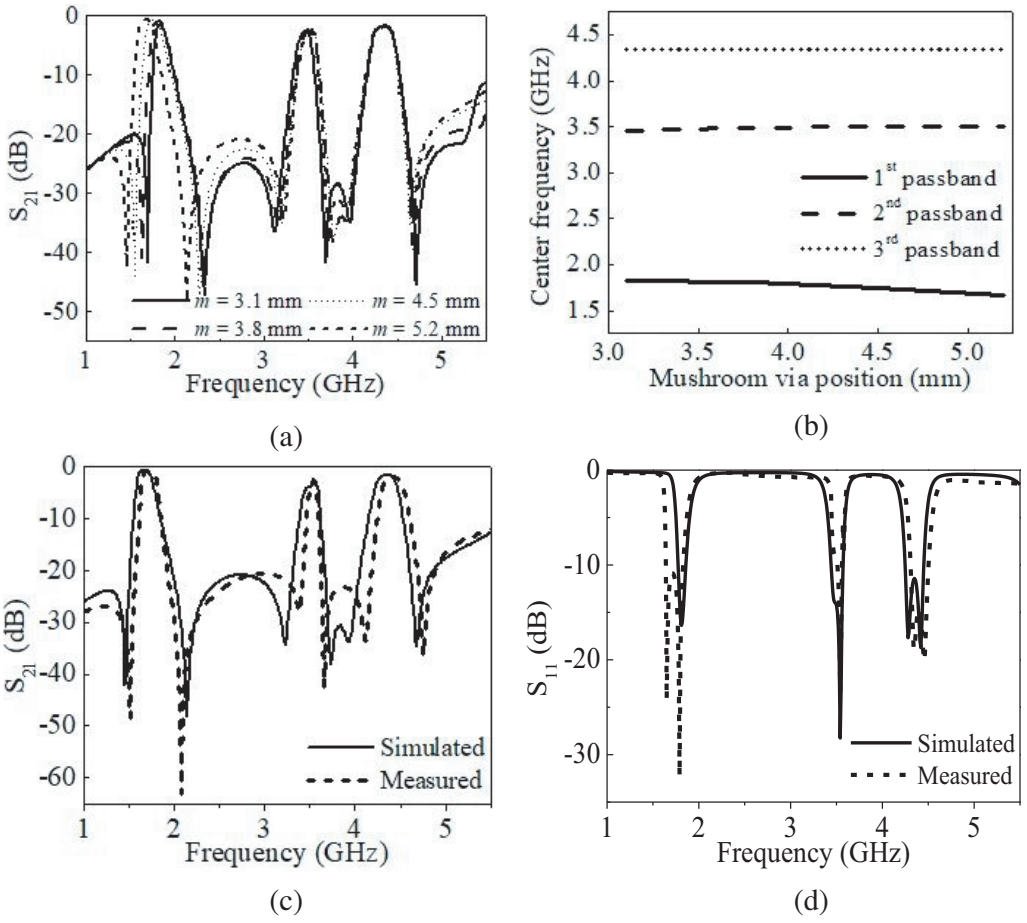

Figure 11. Frequency response and variation in center frequency of 1st passband of triple bandpass filter with inclined displacement of mushroom vias. (a) Frequency response of S_{21}, (b) Variation in center frequency of each passband w.r.t inclined displacement of mushroom vias, (c) Comparison between the simulated and measured S_{21} and (d) comparison between the simulated and measured S_{11} responses for mushroom vias displaced by $m = 5.2\,\text{mm}$.

is shown in Figure 11(a). As it is clear through the electric field distributions shown in Figure 9, such displacements of mushroom via disturb only the fundamental mode; therefore, the CF of the 1st passband shifts to lower values due to the increased mushroom via displacement as presented in the frequency response characteristics in Figure 11(a). The 2nd and 3rd passbands remain almost undisturbed. It is clear from Figure 11(a) that an inclined displacement of mushroom via, m, from 3.1 mm to 5.2 mm shifts the CF of the 1st passband from 1.81 GHz to 1.66 GHz, i.e., nearly a 8.3% shift in CF of the 1st passband. A profile of the resonance frequency of each passband with respect to regular displacement of mushroom vias is shown in Figure 11(b). The CF of the 1st passband decreases as the mushroom via shifts from mean position towards the margin, but the CFs of other two passbands remain constant which is clear in Figure 11(b). The frequency characteristics in Figure 11(a) show that the TZs from TZ_3 to TZ_6 also remain fixed, while only TZ_1 and TZ_2 shift accordingly. The study of electric fields distributions and the frequency response characteristics confirm the way to control the fundamental mode by regular displacement of mushroom vias in an inclined direction. The simulated and measured frequency responses of S_{21} and S_{11} of this triple bandpass filter with displaced mushroom vias are shown in Figure 11(c) and Figure 11(d) respectively which shows a descent agreement. Thus the CF of the 1st passband can be shifted, and a control over the 1st passband is established without disturbing the 2nd and 3rd passbands.

3.1.2. Control over 1st Passband by Varying Diameter of Mushroom Vias

The structure of the proposed filter with general schematic, having shift in via by p, rotation by angle θ and via diameters $d_1 = d_2 = 0.8$ mm is shown in Figure 12(a), and the fabricated sample of the filter structure with via diameters $d_1 = d_2 = 0.6$ mm is shown in Figure 12(b).

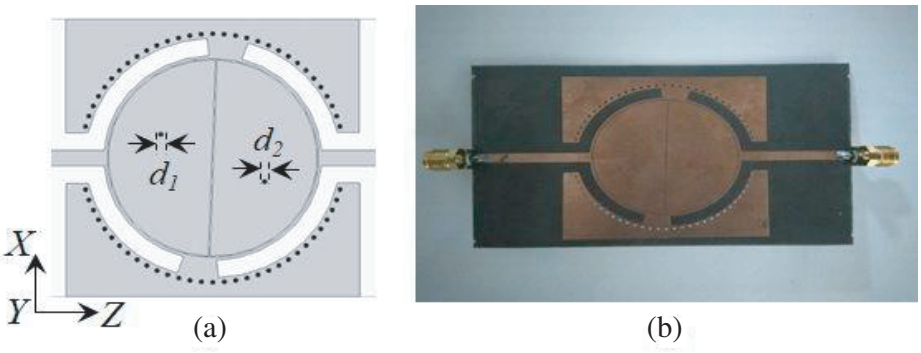

Figure 12. Schematic of the filter structure with varying diameter of mushroom vias. (a) The modeled filter structure. (b) The fabricated sample.

The corresponding electric fields distributions of the three excited modes, which are employed to generate three passbands, are shown in Figure 7(a), Figure 7(b), and Figure 7(c). This electric field distributions help to realize that a change in mushroom via diameters, d_1 and d_2, would disturb the field distributions of fundamental mode (TM_{101}), but the electric field distributions of the higher modes (TM_{201odd} and $TM_{201even}$) are hardly affected because the mushroom vias lie on the null region of field distributions. As the via diameters, d_1 and d_2, increase from 0.6 mm to higher values, the electric field intensity is forcefully pushed towards the mushroom boundary which reduces the surface area of the resonating patch of the mushroom resonators. This reduction in surface area of the resonating patch would increase the frequency of resonance of the fundamental mode (TM_{101}). This increase in via diameters in no way disturbs the electric field distributions of TM_{201odd} and $TM_{201even}$ modes because the positions of these mushroom vias are exactly in the null region of TM_{201odd} and $TM_{201even}$ modes. This study of electric field distributions with varying diameter of the mushroom vias helps to realize the control over the CF of 1st passband keeping 2nd and 3rd passbands as they are. Figure 13(a) and Figure 13(b) present the frequency response characteristics and the profile of the center frequencies of the passbands with respect to different mushroom via diameters, respectively. The frequency response

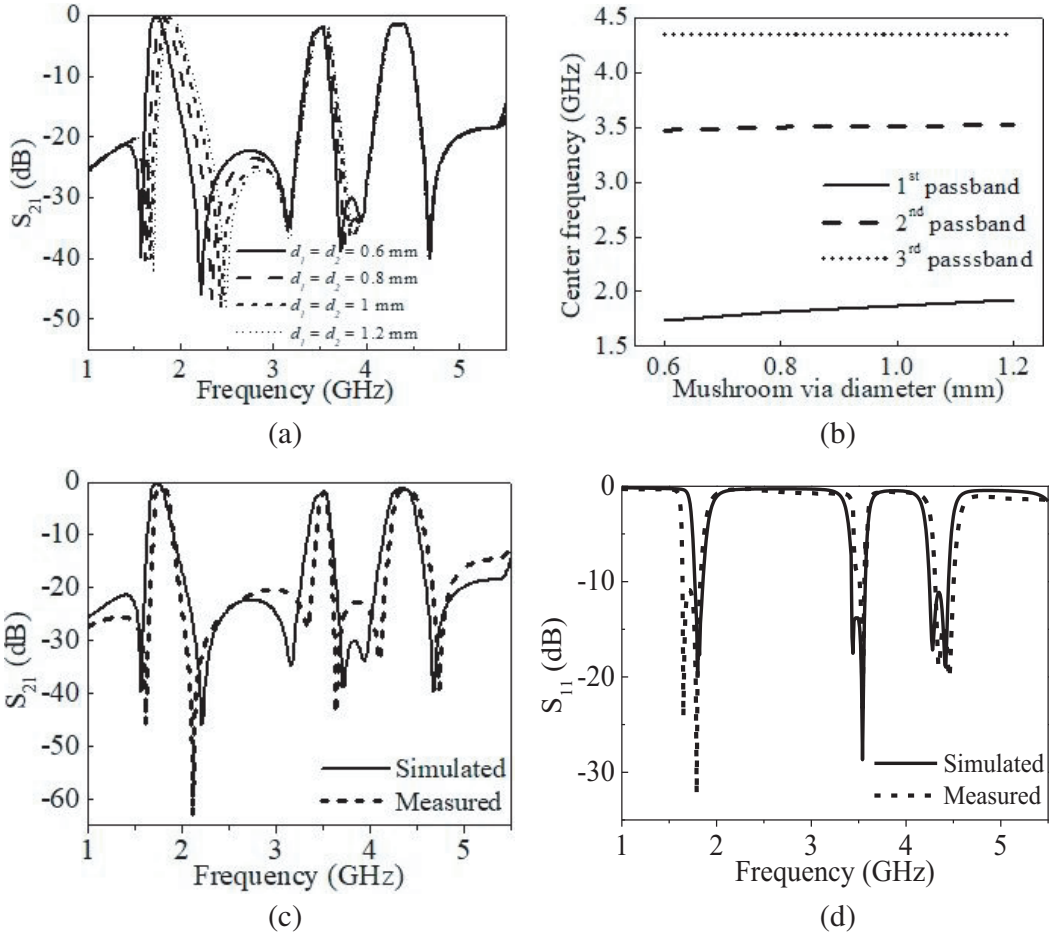

Figure 13. Frequency response and variation in center frequency of 1st passband of triple bandpass filter with varying diameters of mushroom vias. (a) Frequency response of S_{21}, (b) Variation in center frequency of each passband w.r.t varying diameters of mushroom vias, (c) Comparison between the simulated and measured S_{21} and (d) comparison between the simulated and measured S_{11} responses for mushroom via diameters, $d_1 = d_2 = 0.6\,\text{mm}$.

characteristics shown in Figure 13(a) depicts that the CF of the 1st passband shifts from lower frequency to higher frequency when the via diameters, d_1 and d_2, increase, and it is also evident that the 2nd and 3rd passbands remain unchanged with no shift in their respective CFs. Figure 13(a) shows that a change in mushroom via diameter from 0.6 mm to 1.2 mm shifts the CF of the 1st passband from 1.74 GHz to 1.95 GHz, i.e., nearly a shift in 10.5%. As the 1st passband only shifts to higher frequency due to the increase in mushroom via diameters, correspondingly the profile of passband CFs shown in Figure 13(b) shows the rise in resonance frequency of the 1st passband w.r.t mushroom via diameter, whereas CFs of other passbands remain constant as observed in Figure 13(b). The simulated and measured frequency responses of S_{21} and S_{11} of this triple bandpass filter with mushroom via diameter $d_1 = d_2 = 0.6\,\text{mm}$ are compared and shown in Figure 13(c) and Figure 13(d), respectively. Both responses fairly agree to each other with slight discrepancy which can be attributed to fabrication inaccuracies. Consequently, the resonating mode of the 1st passband and thereon the CF of the 1st passband can be controlled by varying the via diameter of the mushroom resonator.

Therefore, two distinct ways are established here to control the CF of the 1st passband, firstly by displacing the mushroom vias in an inclined direction and secondly by varying the mushroom via diameters. Both the 2nd and 3rd passbands are kept undisturbed in these two methods of control over the 1st passband.

3.2. Control over 2nd Passband

Two separate methodologies are proposed in this paper to control the 2nd passband of this triple bandpass filter. Perturbation of surface current distributions and electric field distributions by loading longitudinal perturbation slots and CSRRs into the cavity appears as simple ways to control the corresponding excited mode which are responsible for the generation of the 2nd passband.

3.2.1. Control over 2nd Passband Using Perturbation Slots

The surface current distributions of the triple bandpass filter, shown in Figure 7(d), Figure 7(e), and Figure 7(f) help to realize that if a linear slot of length, l_1, and thickness, t_1, is loaded into each ScMR of the filter structure as shown in Figure 14(a), the surface current of mode 2 (TM_{201odd}) is perturbed by deviating electric path length. Figure 14(b) shows a fabricated sample of the filter structure with perturbation slots of length, $l_1 = 4.5$ mm loaded into the ScMRs. As the electric path lengths of mode 1 (TM_{101}) are linearly aligned to the loaded perturbation slot, so no deviation in electric path length is observed, mode 1 remains unperturbed. Even no disturbance is observed in the surface current distribution of $TM_{201even}$ mode. This is quite clear in Figure 15 where the electric field and surface current distributions of the filter structure loaded with perturbation slots are presented. The more the increase is in slot length, the more the deviation is in path length of the surface current for TM_{201odd} mode as shown in Figure 15(e). Therefore, the method to load a linear slot in mushroom resonator helps to establish the control over TM_{201odd} mode without disturbing the TM_{101} and $TM_{201even}$ modes.

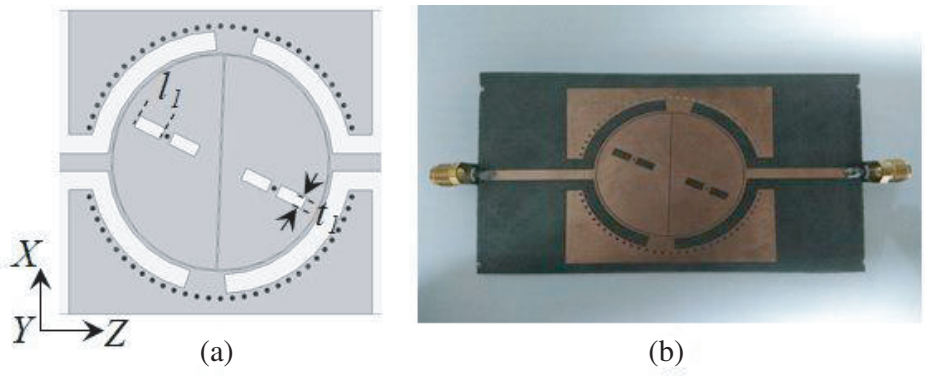

Figure 14. Schematic of the filter structure with loaded perturbation slots. (a) The modeled filter structure. (b) The fabricated sample.

Consequently, the method to independently control the 2nd excited mode (TM_{201odd}) using the loaded perturbation slot helps to establish the control over CF of the 2nd passband. Figure 16(a) and Figure 16(b) show the frequency response characteristics and the profile of the center frequencies of the passbands respectively with respect to different lengths of the loaded perturbation slots. As the method to independently control the 2nd excited mode is established, Figure 16(a) shows the frequency characteristics where the CF of the 2nd passband varies due to the change in length of the perturbation slot. As the slot length l_1 increases from 2.5 mm to 5.5 mm, the surface current path diverges more with an increased electric path length for odd mode 2 (TM_{201odd}), which results in decrease in the resonance frequency of the 2nd passband leading to a shift in CF of the 2nd passband by 3%. During the variation of slot length l_1, mode 1 (TM_{101}) and even mode 2 ($TM_{201even}$) remain undisturbed, and consequently the CFs of 1st and 3rd passbands remain almost at the same value as shown in Figure 16(a). Figure 16(b) shows the profile of CFs of three passbands with respect to the variation in perturbation slot length, where the CF of the 2nd passband falls down as the slot length (l_1) increases, but the CFs of the 1st and 3rd passbands remain nearly constant. The simulated and measured frequency responses of S_{21} and S_{11} of this triple bandpass filter with perturbation slot length, $l_1 = 4.5$ mm, are shown in Figure 16(c) and Figure 16(d), respectively. Both responses fairly agree to each other with slight discrepancies due to fabrication inaccuracies.

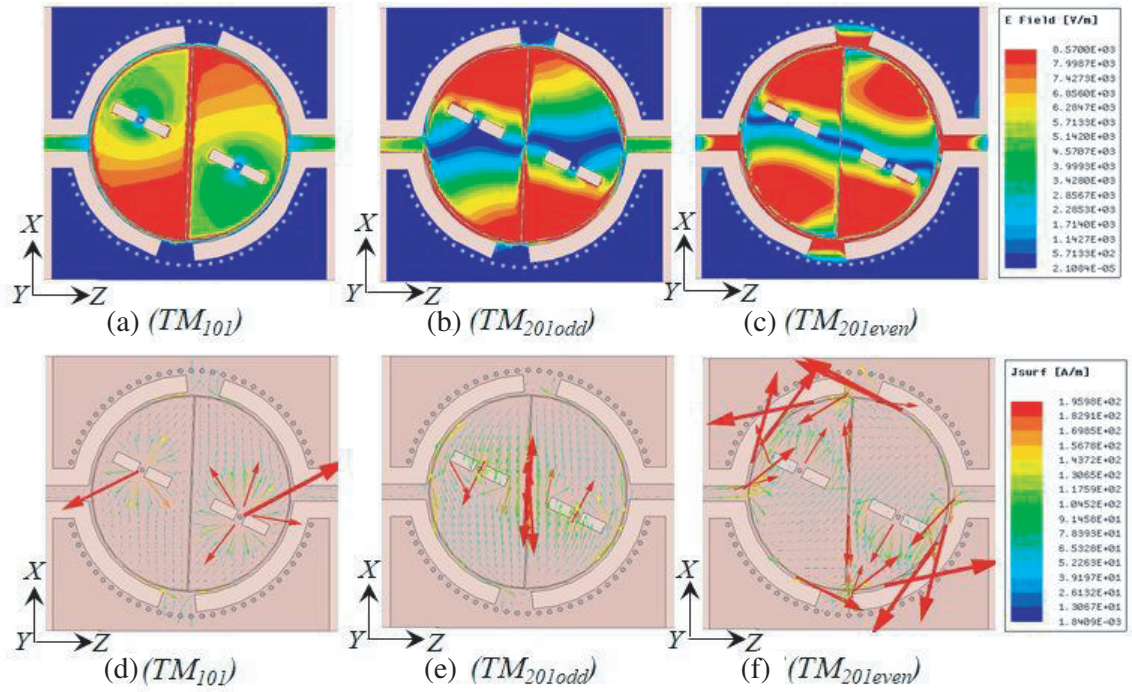

Figure 15. Electric field distributions and surface current distributions of the triple bandpass filter structure loaded with perturbation slots. (a) Electric field distribution at TM_{101} mode, (b) Electric field distribution at TM_{201odd} mode, (c) Electric field distribution at $TM_{201even}$ mode, (d) Surface current distributions at TM_{101} mode, (e) Surface current distribution at TM_{201odd} mode and (f) Surface current distribution at $TM_{201even}$ mode.

3.2.2. Control over 2nd Passband Using CSRRs

A CSRR acts like a parallel LCR resonant circuit, and it strongly couples with the etched out metallic surface when the split gaps of the CSRR are placed exactly in the region of maximum intensity of the electric field distributions of the metal surface [42]. Henceforth, the resonance frequency of the excited mode can be varied only by changing the dimensions of the CSRR. Figure 17(a) shows the schematic of the triple bandpass filter loaded with four single ring rectangular CSRRs with double splits, and Figure 17(b) shows the two SRRs out of all four which are etched out from the metal patch of the loaded mushroom resonators to load the CSRRs. Figure 17(c) shows the fabricated sample with loaded CSRRs into the ScMRs, with CSRR parameters $a = 3\,\text{mm}$, $b = 8\,\text{mm}$, $g_1 = 0.5\,\text{mm}$, and $c_1 = 0.5\,\text{mm}$. The loaded CSRRs are oriented in such a way that the split gaps of each ring lie at the region of maximum intensity of the electric field distributions at TM_{201odd} mode, which is clear in Figure 18. The loaded CSRRs being normal to the magnetic field of the excited electromagnetic wave result in some induced current along the split ring which governs the resonance frequency of the excited TM_{201odd} mode. Thus, the resonance frequency of TM_{201odd} mode can be controlled just by varying the dimensions of the loaded CSRRs. A change in the width of the loaded CSRRs affects the self-resonance frequency of the equivalent LCR circuit. As the width increases, the effective electrical length of the CSRR increases as well. Consequently, the equivalent inductance of the LCR circuit increases which reduces the resonant frequency.

Figure 19(a) shows the downward shift in the CF of the 2nd passband when the widths of CSRRs increase, but the 1st and 3rd passbands remain undisturbed. Figure 19(b) shows the profile of CFs of three passbands with respect to the change in the width of the CSRRs, which shows the decrease in CF of the 2nd passband due to the increase in the width of CSRRs that too keeps the 1st and 3rd passband constant. The same concept can be practiced to control the 2nd passband CF by varying the length of the loaded CSRRs, which is illustrated in the frequency response in Figure 20(a) and the CF profile of each

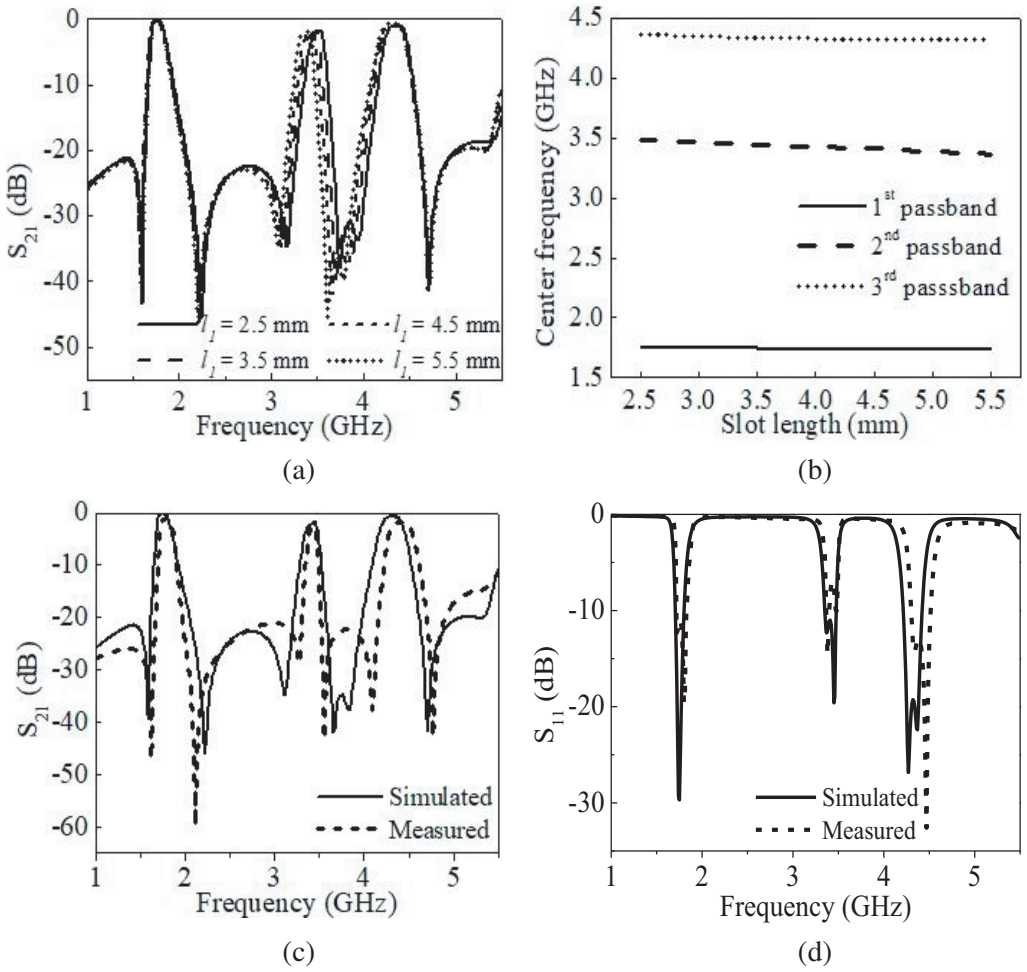

Figure 16. Frequency response and variation in center frequency of 2nd passband of triple bandpass filter with varying length of perturbation slot. (a) Frequency response of S_{21}, (b) Variation in center frequency of each passband w.r.t varying length of perturbation slots, (c) Comparison between the simulated and measured S_{21} and (d) comparison between the simulated and measured S_{11} responses for perturbation slot length, $l_1 = 4.5\,\text{mm}$.

passband shown in Figure 20(b). When the split gap, g_1, of the loaded CSRRs is increased, the effective electrical length of the CSRRs decreases, and the resonance frequency increases. Consequently, the CF of the 2nd passband increases as presented in the frequency response in Figure 21(a). Figure 21(b) shows the profile of the CFs of the three passbands with respect to the variation in split gap, g_1. The more the split gap is, the more the rise is in the CF of the 2nd passband keeping CFs of the other two passbands constant. Figure 22 presents the simulated and measured frequency responses of S_{21} and S_{11} of the proposed filter structure with loaded CSRRs, where the measured responses agree fairly with the simulated responses.

3.3. Control over 3rd Passband

A separate technique is proposed here in order to control the 3rd passband of the proposed triple-band bandpass filter without disturbing the 1st and 2nd passbands. As explained earlier the even mode of TM_{201}, i.e., $\text{TM}_{201even}$, is responsible for the generation of the 3rd passband. The 3rd passband and the selectivity of the falling edge are controlled by source to load coupling. Figure 7(c) shows some strong intensity of the electric field distributions between the two extended perturbation slots. The variation of electric field distributions at this region governs the control over $\text{TM}_{201even}$ mode.

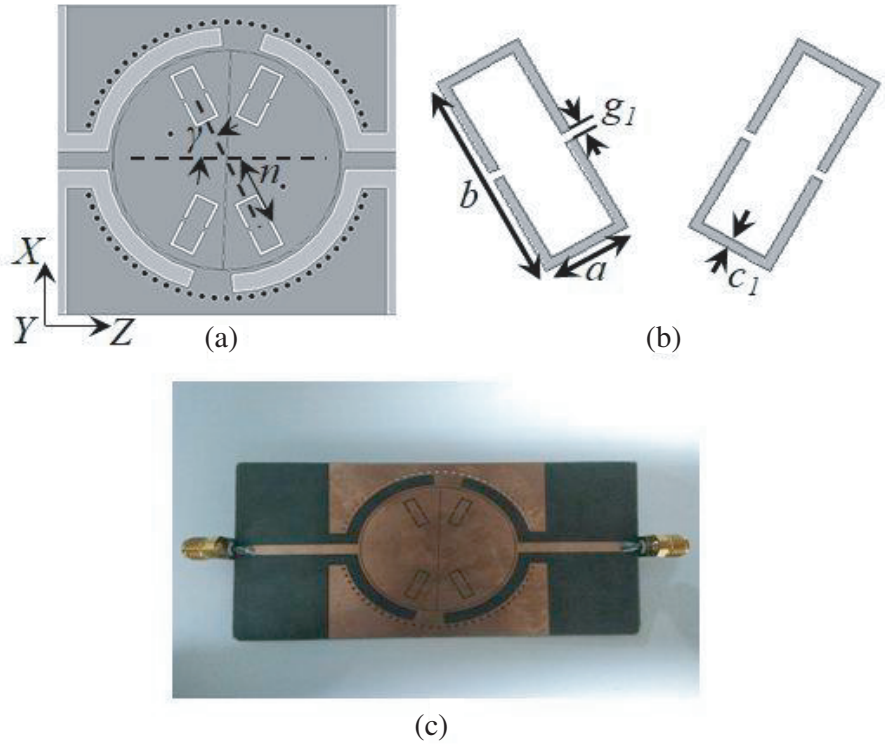

Figure 17. Schematic of the filter structure loaded with four single ring rectangular CSRRs. (a) The triple bandpass filter structure loaded with four single ring rectangular CSRRs. (b) The schematic of two SRRs to be etched out from the metal patch of the mushroom resonator. (c) The fabricated sample with CSRR parameters, $a = 3\,\text{mm}$, $b = 8\,\text{mm}$, $g_1 = 0.5\,\text{mm}$ and $c_1 = 0.5\,\text{mm}$.

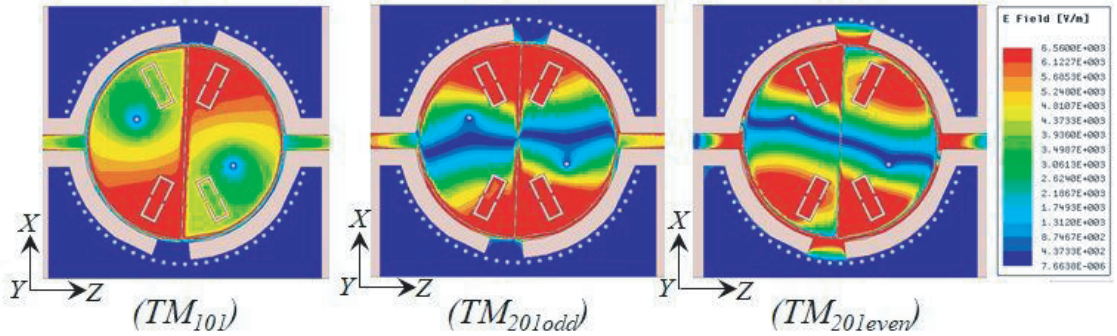

Figure 18. Electric field distributions of the filter structure with loaded CSRRs.

Therefore, this concept could be helpful to establish the control over the 3rd passband. The angular difference between the two perturbation slots of the proposed triple bandpass filter is denoted by φ as presented in Figure 3(d). The optimized value of the angular difference between two perturbation slots is $\varphi = 25.7°$. As φ increases the angular separation between two perturbation slots increases which simultaneously reduces the electric coupling strength between the source and load and also disturbs the second cross coupling. Figure 23(a) and Figure 23(b) show the schematic of the filter structure and the corresponding fabricated sample with $\varphi = 27.7°$. The more the φ increases, the closer the two TZs, TZ_4 and TZ_5, come to each other. Additionally, the last transmission zero of the entire passband, i.e., TZ_6, shifts to higher frequencies with reduced selectivity. This phenomenon is illustrated clearly in Figure 24(a). As φ increases, the change in the coupling strength shifts the CF of the 3rd

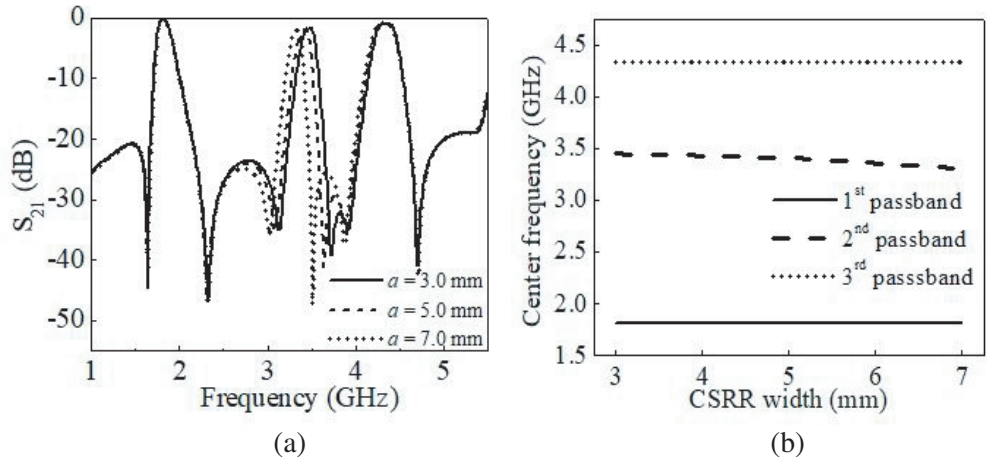

Figure 19. Frequency response and variation in center frequency of 2nd passband of triple bandpass filter with varying width of CSRRs. (a) Frequency response of S_{21}. (b) Variation in center frequency of each passband w.r.t varying width of CSRRs.

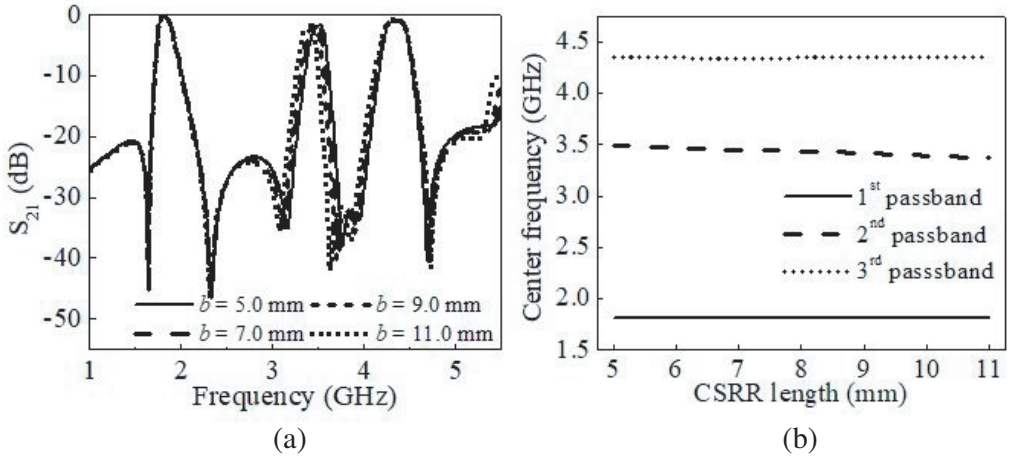

Figure 20. Frequency response and variation in center frequency of 2nd passband of triple bandpass filter with varying length of CSRRs. (a) Frequency response of S_{21}. (b) Variation in center frequency of each passband w.r.t varying length of CSRRs.

passband to higher value. Figure 24(a) shows that an increase in φ by 6° increases the CF of the 3rd passband by nearly 6.6%, keeping other two passbands completely undisturbed. The profiles of CFs of three passbands with respect to variation in angular difference between two radial slots are shown in Figure 24(b). The increase in angle φ reduces the source to load coupling which affects the CF of the 3rd passband by shifting it to higher values, whereas the 1st and 2nd passbands remain undisturbed. The simulated and measured frequency responses of S_{21} and S_{11} are compared in this case and presented in Figure 24(c) and Figure 24(d), respectively, which shows descent agreement as well.

After establishing this technique of independent control over the passbands of the proposed triple-band bandpass filter, a comparative study is carried out as listed in Table 1. It highlights the changes applied in the controlling parameters in order to independently control the excited modes which are responsible for the generation of each passband along with percentage change in the center frequency of each passband.

Table 2 shows a comparison between the results of independent center frequency controlling technique established in the proposed triple bandpass filter and other bandpass filters. It shows the achieved development on independent control over the CFs in each passband with high passband

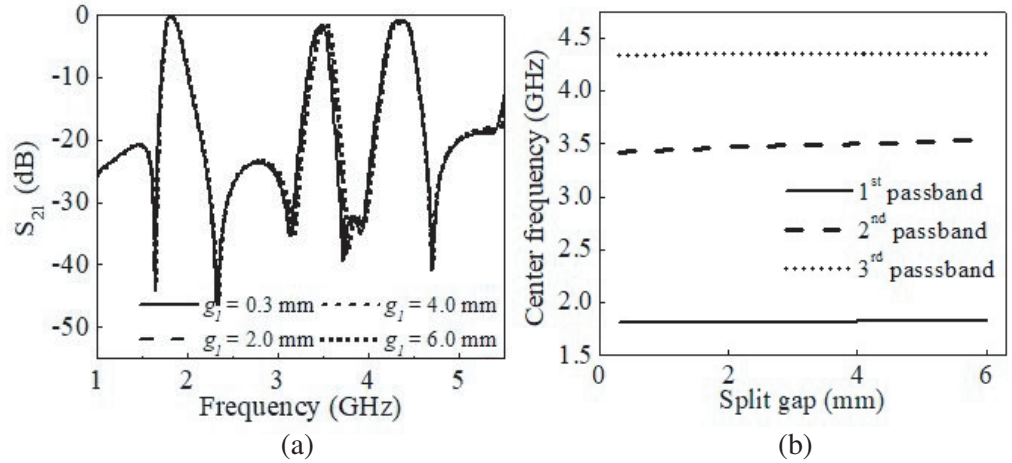

Figure 21. Frequency response and variation in center frequency of 2nd passband of triple bandpass filter with varying split gap of CSRRs. (a) Frequency response of S_{21}. (b) Variation in center frequency of each passband w.r.t varying split gap of CSRRs.

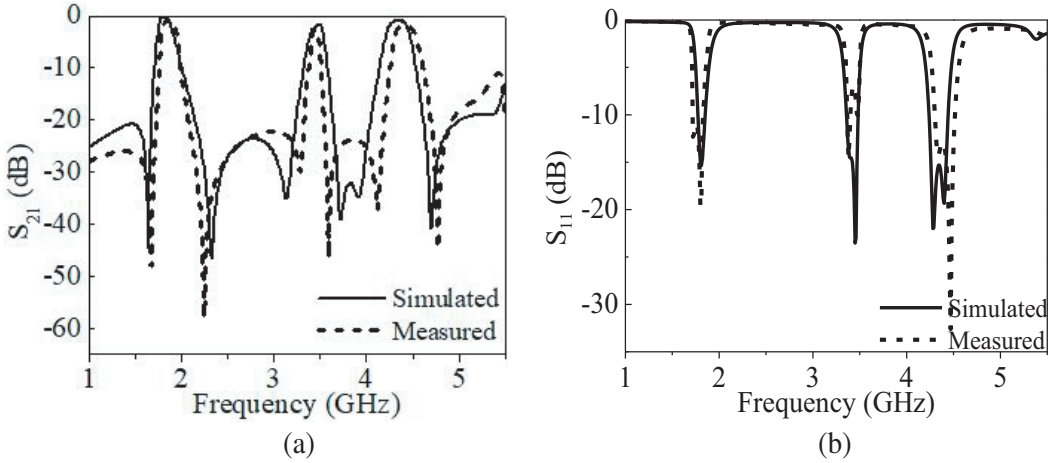

Figure 22. Comparison between the simulated and measured frequency responses of (a) S_{21} and (b) S_{11} for CSRR loaded mushroom resonators inside CSIW with, $a = 3\,\text{mm}$, $b = 8\,\text{mm}$, $g_1 = 0.5\,\text{mm}$ and $c_1 = 0.5\,\text{mm}$.

selectivity, comparatively wider FBW, and relatively less insertion loss at the passbands. In the proposed method, the CFs of all three passbands are independently controlled compared to other referred works. In addition, multiple methods are proposed to independently control the CFs of the 1st and 2nd passbands compared to the referred methods in [15, 17, 19, 22, 23, 26–29, 31, 32, 35]. The filter response shows enhanced passband selectivity with six TZs throughout its frequency response compared to [15, 17, 19, 22, 23, 26–32, 35]. Relatively wider FBWs at lower operating frequencies are attained at all three passbands in this CF controlling technique with respect to other referred works operating at higher center frequencies [15, 22, 27, 28 31]. Relatively less area of $(0.38 \times 0.38)\ \lambda_g^2$ is consumed by the proposed filter structure than other referred works [15, 28, 29, 31, 32, 35] which control only one or two passbands, show comparatively poor passband selectivity with less TZs, and undergo higher insertion loss too. The proposed method of independent control over the CFs of three passbands is introduced in the triple bandpass filter which occupies a significantly compact volume of $0.0011\lambda_g^3$ after being modelled and fabricated on a dielectric substrate, RT/Duroid 5880 with dielectric constant, $\varepsilon_r = 2.2$.

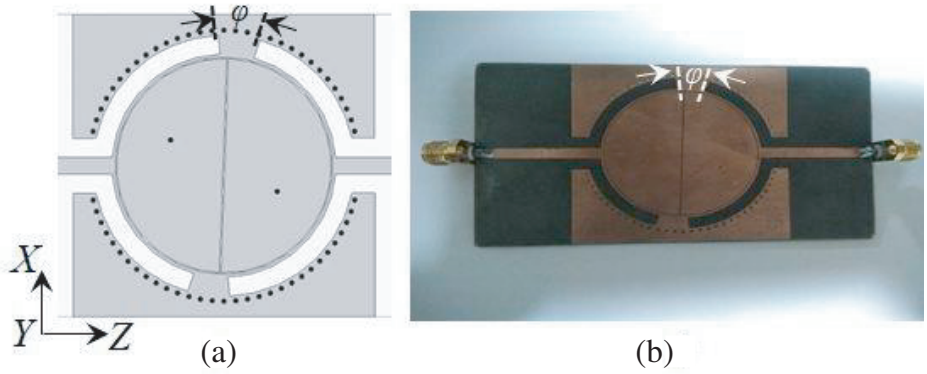

Figure 23. Schematic of the filter structure for controlling the 3rd passband with $\varphi = 27.7°$. (a) The modeled filter structure. (b) The fabricated sample.

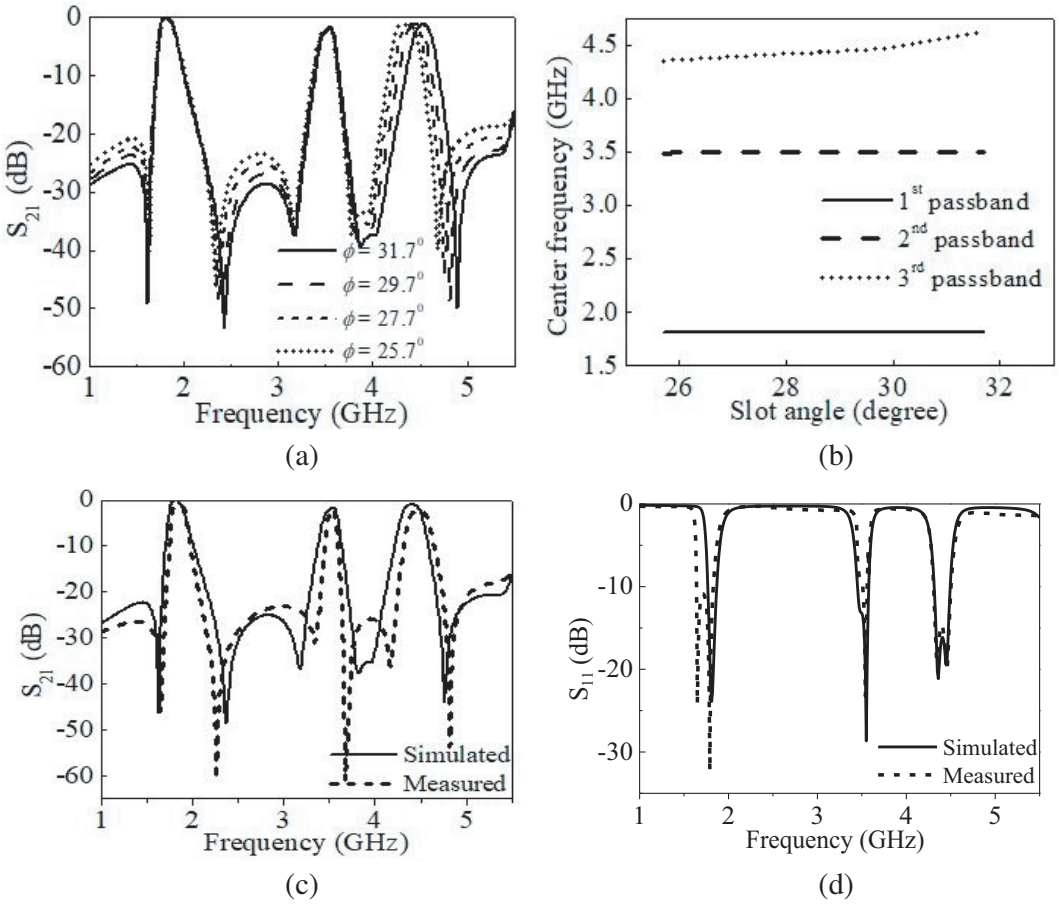

Figure 24. Frequency response and variation in center frequency of 3rd passband of triple bandpass filter with varying angular difference between perturbation slots (φ). (a) Frequency response of S_{21}, (b) Variation in center frequency of each passband w.r.t angular difference between perturbation slots (φ), Comparison between the simulated and measured (c) S_{21} and (d) S_{11} responses for radial perturbation angular difference, $\varphi = 27.7^0$.

Table 1. Controlling parameters and the shift in center frequencies of three passbands.

Controlled modes	Controlling parameters	Change in controlling parameters	Shift in CF (%) of 1st passband	Shift in CF (%) of 2nd passband	Shift in CF (%) of 3rd passband
TM_{101}	Via diameters (d_1 and d_2)	0.6 mm to 1.2 mm	10.5%	No change	No change
	Via displacement (m)	3.1 mm to 5.2 mm	8.3%	No change	No change
TM_{201odd}	Perturbation slot length (l_1)	2.5 mm to 5.5 mm	No change	3%	No change
	CSRR width (a)	3 mm to 7 mm	No change	5.7%	No change
	CSRR length (b)	5 mm to 11 mm	No change	8.5%	No change
	CSRR split gap (g_1)	0.3 mm to 6 mm	No change	3%	No change
$TM_{201even}$	Angular difference (φ)	25.7° to 31.7°	No change	No change	6.6%

Table 2. Comparison with other bandpass filters.

References	CF (GHz) ($f_1/f_2/f_3$)	Order 1st/2nd/3rd band	FBW (%)	Shift in CF (%) of 1st passband	Shift in CF (%) of 2nd passband	Shift in CF (%) of 3rd passband	TZs	IL (dB) 1st/2nd/3rd band	Size ($\lambda_g \times \lambda_g$)
15	5	2	1.7	37%	——	——	2	1.85	1.09 × 1.12
17	1.3	2	——	26%	——	——	0	7	——
19	2.14	2	——	60.8%	——	——	2	3.6	0.19 × 0.11
22	0.8	2	4	52.4%	——	——	0	2.05	——
23	2.26/4.59	2/2	——	36.4%	32.7%	——	2	2.33/3.38	0.196 × 0.155
26	1.2	2	——	17.3%	——	——	2	——	——
27	22.8	2	2.1	10.5%	——	——	0	3.05	——
28	1.4	2	3.7	28%	——	——	0	4	1.19 × 1.7
29	1.4	2	——	28%	——	——	1	2.3	1.0 × 0.7
30	10.75	1	——	1st method-4.56%, 2nd method-5.1%	——	——	0	——	——
31	10	4	8	10%	——	——	0	——	4.65 × 15.78
32	7.62	2	——	4.2%	——	——	2	1.3	1.06 × 1.06
35	7.71/9.64	2/2	5.4/8.1	6.6%	5.5%	——	0	1.9/1.65	0.58 × 0.58
Proposed work	**1.9/3.5/4.4**	**2/2/2**	**9/5/5.8**	**1^{st}method-10.5%, 2^{nd}method-8.3%**	**1^{st} method-3%, 2^{nd} method-5.7%, 3^{rd} method-8.5%, 4^{th} method-3%**	**6.6%**	**6**	**1.5/1.87/1.8**	0.38 × 0.38

4. CONCLUSION

This paper presents a triple-band bandpass filter based on a CSIW cavity loaded with two cascaded ScMRs, and thereafter individual techniques are established to independently control the CFs of the three passbands by introducing mode perturbations and variation in coupling strengths. The electric field distributions and surface current distributions of the top metal layer at each excited modes of the proposed triple-band bandpass filter are studied and thoroughly discussed before dealing with the process of perturbation and variation in source to load coupling strength. Variations in mushroom via diameters, mushroom via positions, loaded perturbation slot length, loaded CSRRs dimensions, and source to load coupling strength are separately utilized to independently control the three excited modes and consequently establish the control over the resonance frequencies of these excited modes. These techniques subsequently help to control the CFs of each passband independently without disturbing the CFs of other passbands. The measured results are in good agreement with the simulated ones, and slight discrepancies which are observed can be attributed to fabrication inaccuracies. Such a compact triple-band bandpass filter with ability to independently control the CFs of each passbands has promising applications in Wi-Fi communications, cellular base stations, and satellite communications.

REFERENCES

1. Deslandes, D. and K. Wu, "Accurate modeling, wave mechanisms, and design considerations of a substrate integrated waveguide," *IEEE Transactions on Microwave Theory and Techniques*, Vol. 54, No. 6, 2516–2526, 2006.
2. Chen, X. P. and K. Wu, "Substrate integrated waveguide filter: Basic design rules and fundamental structure features," *IEEE Microwave Magazine*, Vol. 15, No. 5, 108–116, 2014.
3. Chen, X. P. and K. Wu, "Substrate integrated waveguide filters: Design techniques and structure innovations," *IEEE Microwave Magazine*, Vol. 15, No. 6, 121–133, 2014.
4. Chen, X. P., K. Wu, and Z. L. Li, "Dual-band and triple-band substrate integrated waveguide filters with Chebyshev and quasielliptic responses," *IEEE Transactions on Microwave Theory and Techniques*, Vol. 55, No. 12, 2569–2578, 2007.
5. Wang, H. Y., G. H. Li, Y. D. Wu, W. Yang, and T. Mou, "A novel triple-band filter based on triple-mode substrate integrated waveguide," *Progress In Electromagnetics Research*, Vol. 58, 59–65, 2016.
6. Xie, H. W., K. Zhou, C. X. Zhou, and W. Wu, "Substrate integrated waveguide triple-band bandpass filters using triple-mode cavities," *IEEE Transactions on Microwave Theory and Techniques*, Vol. 66, No. 6, 2967–2977, 2018.
7. Zhou, K., C. Zhou, and W. Wu, "Substrate-integrated waveguide triple-band filter with improved frequency and bandwidth allocations," *Electronics Letters*, Vol. 54, No. 19, 1132–1134, 2018.
8. Zhou, K., C. X. Zhou, H. W. Xie, and W. Wu, "Synthesis design of SIW multiband bandpass filters based on dual-mode resonances and split-type dual-and triple-band responses," *IEEE Transactions on Microwave Theory and Techniques*, Vol. 67, No. 1, 151–161, 2018.
9. Tomassoni, C., L. Silvestri, M. Bozzi, and L. Perregrini, "Substrate-integrated waveguide filters based on mushroom-shaped resonators," *International Journal of Microwave and Wireless Technologies*, Vol. 8, Nos. 4–5, 741–749, 2016.
10. Awasthi, S., A. Biswas, and M. Jaleel Akhtar, "A CAD model of triple bandpass filter implemented with mushroom structure," *International Journal of RF and Microwave Computer-Aided Engineering*, Vol. 24, No. 4, 421–428, 2014.
11. Chaudhury, S. S., S. Awasthi, and R. K. Singh, "Dual band bandpass filter based on substrate integrated waveguide loaded with mushroom resonators," *Microwave and Optical Technology Letters*, Vol. 62, No. 6, 2226–2235, 2020.
12. Chaudhury, S. S., S. Awasthi, and R. K. Singh, "Independent control over resonating modes of mushroom resonator loaded substrate integrated waveguide using perturbation slots," *2019 IEEE Indian Conference on Antennas and Propagation (InCAP)*, 1–4, IEEE, 2019.
13. Wu, Y., Y. Chen, L. Jiao, Y. Liu, and Z. Ghassemlooy, "Dual-band dual-mode substrate integrated waveguide filters with independently reconfigurable TE_{101} resonant mode," *Scientific Reports*, Vol. 6, No. 1, 1–10, 2016.
14. Lee, T. H., B. Lee, S. Nam, Y. S. Kim, and J. Lee, "Frequency-tunable tri-function filter," *IEEE Transactions on Microwave Theory and Techniques*, Vol. 65, No. 11, 4584–4592, 2017.
15. Zhang, Q. L., S. Adhikari, B. Z. Wang, and K. Wu, "A reconfigurable dual-mode bandpass filter based on substrate integrated waveguide," *Microwave and Optical Technology Letters*, Vol. 59, No. 4, 934–937, 2017.
16. Hinojosa, J., A. Saura-Ródenas, A. Alvarez-Melcon, and F. L. Martínez-Viviente, "Reconfigurable Coplanar Waveguide (CPW) and Half-Mode Substrate Integrated Waveguide (HMSIW) bandstop filters using a varactor-loaded metamaterial-inspired open resonator," *Materials*, Vol. 11, No. 1, 39, 2018.
17. You, B., S. Lu, L. Chen, and Q. J. Gu, "A half-mode substrate integrated filter with tunable center frequency and reconfigurable bandwidth," *IEEE Microwave and Wireless Components Letters*, Vol. 26, No. 3, 189–191, 2016.

18. Guo, J., B. You, and G. Q. Luo, "A miniaturized eighth-mode substrate-integrated waveguide filter with both tunablecenter frequency and bandwidth," *IEEE Microwave and Wireless Components Letters*, Vol. 29, No. 7, 450–452, 2016.
19. Lan, B., C. Guo, and J. Ding, "A fully tunable two-pole bandpass filter with wide tuning range based on half mode substrate integrated waveguide," *Microwave and Optical Technology Letters*, Vol. 60, No. 4, 865–870, 2018.
20. Iqbal, A., J. J. Tiang, C. K. Lee, N. K. Mallat, and S. W. Wong, "Dual-band half mode substrate integrated waveguide filter with independently tunable bands," *IEEE Transactions on Circuits andSystems II: Express Briefs*, Vol. 67, No. 2, 285–289, 2019.
21. Sam, S. and S. Lim, "Tunable band-pass filters based on varactor-loaded complementary split-ring resonators on half-mode substrate integrated waveguide," *Microwave and Optical Technology Letters*, Vol. 55, No. 10, 2458–2460, 2013.
22. Anand, A., J. Small, D. Peroulis, and X. Liu, "Theory and design of octave tunable filters with lumped tuning elements," *IEEE Transactions on Microwave Theory and Techniques*, Vol. 61, No. 12, 4353–4364, 2013.
23. Zhou, C. X., C. M. Zhu, and W. Wu, "Tunable dual-band filter based on stub-capacitor-loaded half-mode substrate integrated waveguide," *IEEE Transactions on Microwave Theory and Techniques*, Vol. 65, No. 1, 147–155, 2016.
24. Zhao, D. and L. Li, "A dual-mode SIW filter with tunable frequency, reconfigurable bandwidth and adjustable transmission zero," *2018 International Applied Computational Electromagnetics Society Symposium-China (ACES)*, 1–2, IEEE, Jul. 29, 2018.
25. Li, L., D. Zhao, J. Bai, Q. Wang, and Z. Lei, "A tunable third-order bandpass filter based on combining dual-mode square shaped substrate integrated waveguide resonator with triangular shaped resonator," *International Journal of RF and MicrowaveComputer-Aided Engineering*, Vol. 29, No. 1, e21454, 2019.
26. Nam, S., B. Lee, and J. Lee, "Reconfigurable bandpass filter topology using cul-de-sac resonators with adjustable notches," *2016 IEEE MTT-S International Microwave Symposium (IMS)*, 1–4, IEEE, May 22, 2016.
27. Lee, B., S. Nam, B. Koh, C. Kwak, and J. Lee, "K-band frequency tunable substrate-integrated-waveguide resonator filter with enhanced stopband attenuation," *IEEE Transactions on Microwave Theory and Techniques*, Vol. 63, No. 11, 3632–3640, 2015.
28. Sekar, V., M. Armendariz, and K. Entesari, "A 1.2–1.6-GHz substrate-integrated-waveguide RF MEMS tunable filter," *IEEE Transactions on Microwave Theory and Techniques*, Vol. 59, No. 4, 866–876, 2011.
29. Sekar, V. and K. Entesari, "A half-mode substrate-integrated waveguide tunable filter using packaged RF MEMS switches," *IEEE Microwave and Wireless Components Letters*, Vol. 22, No. 7, 336–338, 2012.
30. Mira, F., J. Mateu, and C. Collado, "Mechanical tuning of substrate integrated waveguide resonators," *IEEE Microwave and Wireless Components Letters*, Vol. 22, No. 9, 447–449, 2012.
31. Mira, F., J. Mateu, and C. Collado, "Mechanical tuning of substrate integrated waveguide filters," *IEEE Transactions on Microwave Theory and Techniques*, Vol. 63, No. 12, 3939–3946, 2015.
32. Zhang, H., W. Kang, and W. Wu, "Balanced bandpass filter with tunable centre frequency based on substrate integrated waveguide technology," *Electronics Letters*, Vol. 54, No. 14, 886–888, 2018.
33. Dong, Y., C. T. Wu, and T. Itoh, "Miniaturised multi-band substrate integrated waveguide filters using complementary split-ring resonators," *IET Microwaves, Antennas & Propagation*, Vol. 6, No. 6, 611–620, 2012.
34. Chaudhury, S. S. and S. Awasthi, "Multiple passband circular cavity substrate integrated waveguide filter using asymmetric complementary split ring resonators," *2017 IEEE Asia Pacific Microwave Conference (APMC)*, 1246–1249, IEEE, Nov. 13, 2017.

35. Azad, A. R. and A. Mohan, "Single-and dual-band bandpass filters using a single perturbed SIW circular cavity," *IEEE Microwave and Wireless Components Letters*, Vol. 29, No. 3, 201–203, 2019.
36. Sievenpiper, D., L. Zhang, R. F. Broas, N. G. Alexopolous, and E. Yablonovitch, "High-impedance electromagnetic surfaces with a forbidden frequency band," *IEEE Transactions on Microwave Theory and Techniques*, Vol. 47, No. 11, 2059–2074, 1999.
37. Tang, H. J., W. Hong, J. X. Chen, G. Q. Luo, and K. Wu, "Development of millimeter-wave planar diplexers based on complementary characters of dual-mode substrate integrated waveguide filters with circular and elliptic cavities," *IEEE Transactions on Microwave Theory and Techniques*, Vol. 55, No. 4, 776–782, 1999.
38. Liu, Q., D. F. Zhou, D. W. Zhang, and D. L. Lv, "SIW bandpass filters in modified box-section scheme with bypass/constant/frequency dependent coupling in diagonal cross-coupling path," *IET Microwaves, Antennas & Propagation*, Vol. 13, No. 5, 559–566, 2019.
39. Rosenberg, U. and S. Amari, "Novel design possibilities for dual-mode filters without intracavity couplings," *IET Microwaves, Antennas & Propagation*, Vol. 12, No. 8, 296–298, 2002.
40. Amari, S. and U. Rosenberg, "Characteristics of cross (bypass) coupling through higher/lower order modes and their applications in elliptic filter design," *IEEE Transactions on Microwave Theory and Techniques*, Vol. 53, No. 10, 3135–3141, 2005.
41. Hong, J. S. and M. J. Lancaster, *Microstrip Filters for RF/Microwave Applications*, John Wiley & Sons, Apr. 7, 2004.
42. Dong, Y., C. T. Wu, and T. Itoh, "Miniaturised multi-band substrate integrated waveguide filters using complementary split-ring resonators," *IET Microwaves, Antennas & Propagation*, Vol. 6, No. 6, 611–620, 2012.